Perceptual Integration for Qualitatively Different 3-D Cues in the Human Brain

Dicle Dövencioğlu[1]*, Hiroshi Ban[1,2]*, Andrew J. Schofield[1], and Andrew E. Welchman[1]

Abstract

■ The visual system's flexibility in estimating depth is remarkable: We readily perceive 3-D structure under diverse conditions from the seemingly random dots of a "magic eye" stereogram to the aesthetically beautiful, but obviously flat, canvasses of the Old Masters. Yet, 3-D perception is often enhanced when different cues specify the same depth. This perceptual process is understood as Bayesian inference that improves sensory estimates. Despite considerable behavioral support for this theory, insights into the cortical circuits involved are limited. Moreover, extant work tested quantitatively similar cues, reducing some of the challenges associated with integrating computationally and qualitatively different signals. Here we address this challenge by measuring fMRI responses to depth structures defined by shading, binocular disparity,

and their combination. We quantified information about depth configurations (convex "bumps" vs. concave "dimples") in different visual cortical areas using pattern classification analysis. We found that fMRI responses in dorsal visual area V3B/KO were more discriminable when disparity and shading concurrently signaled depth, in line with the predictions of cue integration. Importantly, by relating fMRI and psychophysical tests of integration, we observed a close association between depth judgments and activity in this area. Finally, using a cross-cue transfer test, we found that fMRI responses evoked by one cue afford classification of responses evoked by the other. This reveals a generalized depth representation in dorsal visual cortex that combines qualitatively different information in line with 3-D perception. ■

INTRODUCTION

Many everyday tasks rely on depth estimates provided by the visual system. To facilitate these outputs, the brain exploits a range of inputs: from cues related to distance in a mathematically simple way (e.g., binocular disparity, motion parallax) to those requiring complex assumptions and prior knowledge (e.g., shading, occlusion; Burge, Fowlkes, & Banks, 2010; Kersten, Mamassian, & Yuille, 2004; Mamassian & Goutcher, 2001). These diverse signals each evoke an impression of depth in their own right; however, the brain aggregates cues (Landy, Maloney, Johnston, & Young, 1995; Buelthoff & Mallot, 1988; Dosher, Sperling, & Wurst, 1986) to improve perceptual judgments (Knill & Saunders, 2003).

Here we probe the neural basis of integration, testing binocular disparity and shading depth cues that are computationally quite different. At first glance, these cues may appear so divergent that their combination would be prohibitively difficult. However, perceptual judgments show evidence for the combination of disparity and shading (Lovell, Bloj, & Harris, 2012; Lee & Saunders, 2011; Schiller, Slocum, Jao, & Weiner, 2011; Vuong, Domini,

& Caudek, 2006; Doorschot, Kappers, & Koenderink, 2001; Buelthoff & Mallot, 1988), and the solution to this challenge is conceptually understood as a two-stage process (Landy et al., 1995) in which cues are first analyzed quasi-independently followed by the integration of cue information that has been "promoted" into common units (such as distance). Moreover, observers can make reliable comparisons between the perceived depth from shading and stereoscopic, as well as haptic, comparison stimuli (Schofield, Rock, Sun, Jiang, & Georgeson, 2010; Kingdom, 2003), suggesting some form of comparable information.

To gain insight into the neural circuits involved in processing 3-D information from disparity and shading, previous brain imaging studies have tested for overlapping fMRI responses to depth structures defined by the two cues, yielding locations in which information from disparity and shading converge (Nelissen et al., 2009; Georgieva, Todd, Peeters, & Orban, 2008; Sereno, Trinath, Augath, & Logothetis, 2002). Although this is a useful first step, this previous work has not established integration: For instance, representations of the two cues might be collocated within the same cortical area, but represented independently. By contrast, recent work testing the integration of disparity and motion depth cues, indicates that integration occurs in higher dorsal visual cortex (area V3B/kinetic occipital [KO]; Ban, Preston, Meeson, & Welchman, 2012). This suggests a

[1]University of Birmingham, [2]Japan Society for the Promotion of Science
*These authors contributed equally to this work.

candidate cortical locus in which other types of 3-D information may be integrated; however, it is not clear whether integration would generalize to (i) more complex depth structures and/or (ii) different cue pairings.

First, Ban and colleagues (2012) used simple fronto-parallel planes that can suboptimally stimulate neurons selective to disparity-defined structures in higher portions of the ventral (Janssen, Vogels, & Orban, 2000) and dorsal streams (Srivastava, Orban, De Maziere, & Janssen, 2009) compared with more complex curved stimuli. It is therefore possible that other cortical areas (especially those in the ventral stream) would emerge as important for cue integration if more "shape-like" stimuli were presented. Second, it is possible that information from disparity and motion are a special case of cue conjunctions, and thus, integration effects may not generalize to other depth signal combinations. In particular, depth from disparity and from motion have computational similarities (Richards, 1985) and joint neuronal encoding (DeAngelis & Uka, 2003; Anzai, Ohzawa, & Freeman, 2001; Bradley, Qian, & Andersen, 1995) and can, in principle, support

metric (absolute) judgments of depth. In contrast, the 3-D pictorial information provided by shading relies on a quite different generative process that is subject to different constraints and prior assumptions (Thompson, Fleming, Creem-Regehr, & Stefanucci, 2011; Fleming, Dror, & Adelson, 2003; Koenderink & van Doorn, 2003; Mamassian & Goutcher, 2001; Sun & Perona, 1998; Horn, 1975).

To test for cortical responses related to the integration of disparity and shading, we assessed how fMRI responses change when stimuli are defined by different cues (Figure 1A). We used multivoxel pattern analysis (MVPA) to assess the information contained in fMRI responses evoked by stimuli depicting different depth configurations (convex vs. concave hemispheres to the left vs. right of the fixation point). We were particularly interested in how information about the stimulus contained in the fMRI signals changed depending on the cues used to depict depth in the display. Intuitively, we would expect that discriminating fMRI responses should be easier when differences in the depicted depth configuration
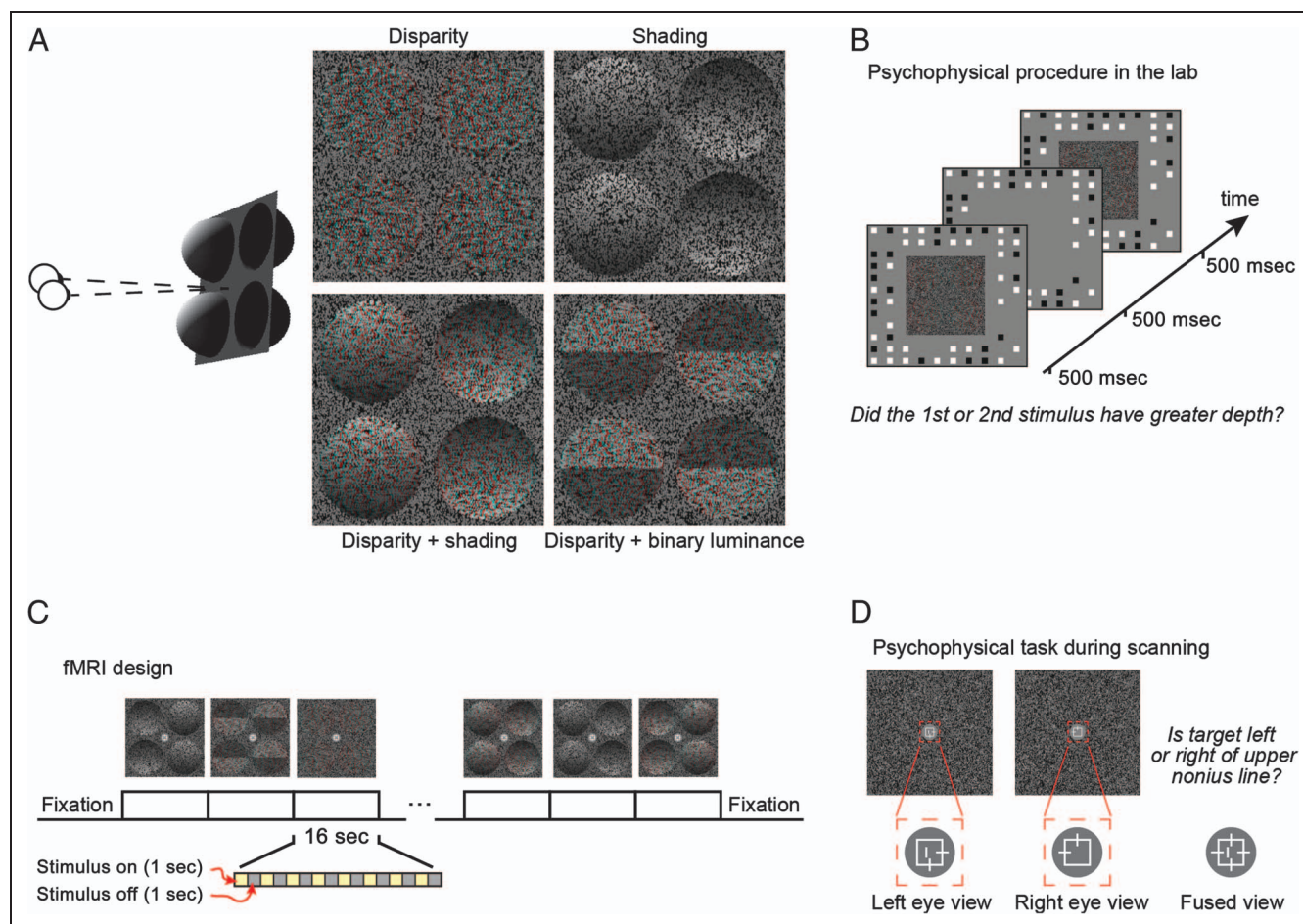

Figure 1. Stimulus illustration and experimental procedures. (A) Left: Cartoon of the disparity and/or shading defined depth structure. One of the two configurations is presented: bumps to the left, dimples to the right. Right: Stimulus examples rendered as red–cyan anaglyphs. (B) Illustration of the psychophysical testing procedure. (C) Illustration of the fMRI block design. (D) Illustration of the vernier task performed by participants during the fMRI experiment. Participants compared the horizontal position of a vertical line flashed (250 msec) to one eye against the upper vertical nonius element of the crosshair presented to the other eye.

were defined by two cues rather than just one (i.e., differences defined by disparity and shading together should be easier to discriminate than differences defined by only disparity). The theoretical basis for this intuition can be demonstrated based on statistically optimal discrimination (Ban et al., 2012), with the extent of the improvement in the two-cue case providing insight into whether the underlying computations depend on the integration of two cues or rather having colocated but independent depth signals.

To appreciate the theoretical predictions for a cortical area that responds to integrated cues versus colocated but independent signals, first consider a hypothetical area that is only sensitive to a single cue (e.g., shading). If shading information differed between two presented stimuli, we would expect neuronal responses to change, providing a signal that could be decoded. By contrast, manipulating a nonencoded stimulus feature (e.g., disparity) would have no effect on neuronal responses, meaning that our ability to decode the stimulus from the fMRI response would be unaffected. Such a computationally isolated processing module is biologically rather unlikely, so next, we consider a more plausible scenario where an area contains different subpopulations of neurons, some of which are sensitive to disparity and others to shading. In this case, we would expect to be able to decode stimulus differences based on changes in either cue. Moreover, if the stimuli contained differences defined by both cues, we would expect decoding performance to improve, where this improvement is predicted by the quadratic sum of the discriminabilities for changes in each cue. This expectation can be understood graphically by conceiving of discriminability based on shading and disparity cues as two sides of a right-angled triangle, where better discriminability equates to longer side lengths; the discriminability of both cues together equals the triangle's hypotenuse whose length is determined based on a quadratic sum (i.e., the Pythagorean equation) and is always at least as good as the discriminability of one of the cues.

The alternative possibility is a cortical region that integrates the depth cues. Under this scenario, we also expect better discrimination performance when two cues define differences between the stimuli. Importantly, however, unlike the independence scenario, when stimulus differences are defined by only one cue, a fusion mechanism is adversely affected. For instance, if contrasting stimulus configurations differ in the depth indicated by shading but disparity indicates no difference, the fusion mechanism combines the signals from each cue with the result that it is less sensitive to the combined estimate than the shading component alone. By consequence, if we calculate a quadratic summation prediction based on MVPA performance for depth differences defined by single cues (i.e., disparity; shading) we will find that empirical performance in the combined cue case (i.e., disparity + shading) exceeds the prediction

(Ban et al., 2012). Here we exploit this expectation to identify cortical responses to integrated depth signals, seeking to identify discrimination performance that is "greater than the sum of its parts" due to the detrimental effects of presenting stimuli in which depth differences are defined in terms of a single cue.

To this end, we generated random dot patterns (Figure 1A) that evoked an impression of four hemispheres, two concave ("dimples") and two convex ("bumps"). We formulated two different types of display that differed in their configuration: (1) bumps left–dimples right (depicted in Figure 1A) versus (2) dimples left–bumps right. We depicted depth variations from (i) binocular disparity, (ii) shading gradients, and (iii) the combination of disparity and shading. In addition, we employed a control stimulus (iv) in which the overall luminance of the top and bottom portions of each hemisphere differed (Ramachandran, 1988; disparity + binary luminance). Perceived depth for these (deliberately) crude approximations of the shading gradients relied on disparity. We tested for integration using both psychophysical and fMRI discrimination performance for the component cues (i, ii) with that for stimuli containing two cues (iii, iv). We reasoned that a response based on integrating cues would be specific to concurrent cue stimulus (iii) and not be observed for the control stimulus (iv).

METHODS

Participants

Twenty observers from the University of Birmingham participated in the fMRI experiments. Of these, five were excluded due to excessive head movement during scanning, meaning that the correspondence between voxels required by the MVPA technique was lost. Excessive movement was defined as ≥4 mm over an 8-min run, and we excluded participants if they had fewer than five runs below this cut-off as there was insufficient data for the MVPA. Generally, participants were able to keep still: The average absolute maximum head deviation relative to the start of the first run for included participants was 1.2 mm versus 4.5 mm for excluded participants. Moreover only one included participant had an average head motion of >2 mm per run, and the mode of the head movement distribution across participants was <1 mm. Six women and nine men were included; 12 were right-handed. Mean age was 26 ± 1.2 (SEM) years. Authors A.E.W. and H.B. participated; all other participants were naive to the purpose of the study. Four of the participants had taken part in Ban et al.'s (2012) study. Participants had normal or corrected-to-normal vision and were prescreened for stereo deficits. Experiments were approved by the University of Birmingham Science and Engineering Ethics Committee; observers gave written informed consent.

Stimuli

Stimuli were random dot stereograms (RDS) that depicted concave or convex hemispheres (radius = 1.7°; depth amplitude, 1.85 cm ≈ 15.7 arcmin) defined by disparity and/or shading (Figure 1A). We used small dots (diameter = 0.06°) and patterns with a high density (94 dots/deg^2) to enhance the impression of shape from shading. We used the Blinn–Phong shading algorithm implemented in MATLAB with both an ambient and a directional light. The directional light source was positioned above the observer at an elevation of 45° with respect to the center of the stimulus, and light was simulated as arriving from optical infinity. The ambient light, and illumination from infinity meant that, for our stimuli, there were no cast shadows. The stimulus was modeled as having a Lambertian surface. For the disparity condition, dots in the display had the same luminance histogram as the shaded patterns; however, their positions (with respect to the original shading gradient) were spatially randomized, breaking the shading pattern. For the shading condition, disparity specified a flat surface. To create the binary luminance stimuli, the luminance of the top and bottom portions of the hemispheres was held constant at the mean luminance of these portions of the shapes for the shaded stimuli. Four hemispheres were presented: two convex, and two concave, located at either side of a fixation marker. Two types of configuration were used: (i) convex on the left, concave on the right and (ii) vice versa. The random dot pattern subtended 8 × 8° and was surrounded by a larger, peripheral grid (18 × 14°) of a black and white squares, which served to provide a stable background reference. Other parts of the display were midgray.

Psychophysics

Stimuli were presented in a laboratory setting using a stereo set-up in which the two eyes viewed separate displays (ViewSonic FB2100x, Walnut, CA) through front-silvered mirrors at a distance of 50 cm. Linearization of the graphics card gray level outputs was achieved using photometric measurements. The screen resolution was 1600 × 1200 pixels at 100 Hz.

Under a two-interval forced-choice design, participants decided which stimulus had the greater depth profile (Figure 1B). On every trial, one interval contained a standard disparity-defined stimulus (±1.85 cm/15.7 arcmin); the other interval contained a stimulus from one of three conditions (disparity alone; disparity + shading; disparity + binary luminance) and had a depth amplitude that was varied using the method of constant stimuli. The shading cue varied as the depth amplitude of the shape was manipulated such that the luminance gradient was compatible with a bump/dimple whose amplitude matched that specified by disparity. Similarly, for the binary luminance case, the stimulus luminance values changed at different depth amplitudes to match the lumi-

nance variations that occurred for the gradient shaded stimuli. The order of the intervals was randomized, and conditions were randomly interleaved. On a given trial, a random jitter was applied to the depth profile of both intervals (uniform distribution within ±1 arcmin to reduce the potential for adaptation to a single disparity value across trials). Participants judged "did the first or second stimulus have greater depth" by pressing an appropriate button. On some runs participants were instructed to consider their judgment relative to the convex portions of the display, in others, the concave portions. The spatial configuration of convex and concave items was randomized. A single run contained a minimum of 630 trials (105 trials × 3 conditions × 2 curvature instructions). We made limited measures of the shading-alone condition as we found in pilot testing that participants' judgments based on shading "alone" were very poor (maximum discriminability in the shading condition was $d' = 0.3 \pm 0.25$), meaning that we could not fit a reliable psychometric function, and participants became frustrated by the seemingly impossible task. Moreover, in the shading-alone condition, stimulus changes could be interpreted as a change of light source direction, rather than depth, given the bas-relief ambiguity (Belhumeur, Kriegman, & Yuille, 1999). This ambiguity should be removed by the constraint from disparity signals in the disparity + shading condition, although this does not necessarily happen (see Discussion).

Imaging

Data were recorded at the Birmingham University Imaging Centre using a 3-T Philips MRI scanner with an eight-channel multiphase array head coil. BOLD signals were measured with an EPI sequence (echo time = 35 msec, repetition time = 2 sec, 1.5 × 1.5 × 2 mm, 28 slices near coronal, covering visual, posterior parietal and posterior temporal cortex) for both experimental and localizer scans. A high-resolution anatomical scan (1 mm^3) was also acquired for each participant to reconstruct cortical surface and coregister the functional data. Following coregistration in the native anatomical space, functional and anatomical data were converted into Talairach coordinates.

During the experimental session, four stimulus conditions (disparity, shading, disparity + shading, disparity + binary luminance) were presented in two spatial configurations (convex on left vs. on right) = 8 trial types. Each trial type was presented in a block (16 sec) and repeated three times during a run (Figure 1C). Stimulus presentation was 1 sec on, 1 sec off, and different random dot stereograms were used for each presentation. These different stimuli had randomly different depth amplitudes (jitter of 1 arcmin) to attenuate adaptation to a particular depth profile across a block. Each run started and ended with a fixation period (16 sec), total duration = 416 sec. Scan sessions lasted 90 min, allowing collection

of 7–10 runs, depending on the initial setup time and each individual participant's requirements for breaks between runs.

Participants were instructed to fixate at the center of the screen, where a square crosshair target (side = 0.5°) was presented at all times (Figure 1D). This was surrounded by a midgray disc area (radius = 1°). A dichoptic Vernier task was used to encourage fixation and provide a subjective measure of eye vergence (Popple, Smallman, & Findlay, 1998). In particular, a small vertical Vernier target was flashed (250 msec) at the vertical center of the fixation marker to one eye. Participants judged whether this Vernier target was to the left or right of the upper nonius line, which was presented to the other eye. We used the method of constant stimuli to vary Vernier target position, and fit the proportion of "target on the right responses" to estimate whether there was any bias in the observers' responses that would indicate systematic deviation from the desired vergence state. The probability of a Vernier target appearing on a given trial was 50%, and the timing of appearance was variable with respect to trial onset (during the first vs. second half of the stimulus presentation), requiring constant vigilance by the participants.

The vernier task was deliberately chosen to ensure that participants were engaged in a task orthogonal to the main stimulus presentations and manipulation. The temporal uncertainty in the timing of presentation and its brief nature ensured participants had to constantly attend to the fixation marker. Thus, differences in fMRI responses between conditions could not be ascribed to attentional state, task difficulty, or the degree of conflict inherent in the different stimuli. Note also that in addition to performing different tasks, the stimuli presented during scanning were highly suprathreshold (i.e., convex vs. concave) to ensure reliable decoding of the fMRI responses. This differed from the psychophysical judgments where we measured sensitivity to small differences in the depth profile of the shapes. We would expect benefits from integrating cues in both cases; however it is important to note these differences imposed by the different types of measurement paradigms (fMRI vs. psychophysics) we have used.

Stereoscopic stimulus presentation was achieved using a pair of video projectors (JVC D-ILA SX21), each containing separate spectral comb filters (INFITEC, GmBH, Ulm, Germany) whose projected images were optically combined using a beam-splitter cube before being passed through a wave guide into the scanner room. The INFITEC interference filters produce negligible overlap between the wavelength emission spectra for each projector, meaning that there is little crosstalk between the signals presented on the two projectors for an observer wearing a pair of corresponding filters. Images were projected onto a translucent screen inside the bore of the magnet. Participants viewed the display via a front-surfaced mirror attached to the headcoil (viewing distance = 65 cm). The two projectors were matched and gray scale linearized using photometric measurements.

Functional and anatomical preprocessing of MRI data was conducted with BrainVoyager QX (BrainInnovation B.V., Maastricht, The Netherlands) and in-house MATLAB routines. For each functional run, data were corrected with slice time correction, 3-D motion correction using trilinear estimation and sync interpolation, high pass filtering, and linear trend removal. After motion correction, each participant's functional data were aligned to their raw 3-D anatomical scan. To transform the data into standardized coordinates, the raw 3-D anatomical images were first transformed to anterior commissure–posterior commissure space using sync interpolation, and then into Talairach space coordinates using sync interpolation. To analyze the functional data in Talairach space, the functional data were transformed by applying the transformation matrices derived for the anatomical data. No spatial smoothing was performed. Retinotopic areas were identified in individual localizer scanning sessions for each participant.

Mapping ROIs

We identified ROIs within the visual cortex for each participant in a separate fMRI session before the main experiment. To identify retinotopically organized visual areas, we used rotating wedge stimuli and expanding/contracting rings to identify visual field position and eccentricity maps (DeYoe et al., 1996; Sereno et al., 1995). Thereby, we identified areas V1, V2 and the dorsal and ventral portions of V3 (which we denote V3d and V3v). Area V4 was localized adjacent to V3v with a quadrant field representation (Tootell & Hadjikhani, 2001), whereas V3A was adjacent to V3d with a hemifield representation. Area V7 was identified as anterior and dorsal to V3A with a hemifield representation (Tyler, Likova, Chen, Kontsevich, & Wade, 2005; Tootell et al., 1998). The borders of area V3B were identified as based on a hemifield retinotopic representation inferior to and sharing a foveal representation with V3A (Tyler et al., 2005). This retinotopically defined area overlapped with the contiguous voxel set that responded significantly more ($p = 10^{-4}$) to intact versus scrambled motion-defined contours which has previously been described as the KO area (Zeki, Perry, & Bartels, 2003; Dupont et al., 1997). Given this overlap, we denote this area as V3B/KO (Ban et al., 2012; see also Larsson, Heeger, & Landy, 2010). Talairach coordinates for this area are provided in Table 1. We identified the human motion complex (hMT$^+$/V5) as the set of voxels in the lateral temporal cortex that responded significantly more ($p = 10^{-4}$) to coherent motion than static dots (Zeki et al., 1991). Finally, the lateral occipital complex was defined as the voxels in the lateral occipito-temporal cortex that responded significantly more ($p = 10^{-4}$) to intact versus scrambled images of objects (Kourtzi & Kanwisher, 2001). The posterior subregion lateral occipital (LO)

Table 1. Talairach Space Coordinates of the Centroids of the Region We Denote V3B/KO

	Left Hemisphere			Right Hemisphere		
	x	y	z	x	y	z
V3B/KO (all participants)						
Mean	−27.5	−84.7	7.0	31.6	−80.7	6.5
SD	4.4	4.3	3.9	4.1	4.4	4.8
Good integrators						
Mean	−26.9	−86.0	6.7	31.5	−81.7	7.2
SD	4.2	4.2	4.2	4.0	4.5	4.8
Poor integrators						
Mean	−28.1	−83.4	7.2	31.8	−79.9	5.8
SD	4.6	4.4	3.7	4.1	4.4	4.8

We present data for all participants and participants separated into good and poor integration groups.

extended into the posterior inferiotemporal sulcus and was defined based on functional activations and anatomy (Grill-Spector, Kushnir, Hendler, & Malach, 2000).

MVPA

To select voxels for the MVPA, we used a participant-by-participant fixed effects general linear model (GLM) across runs on gray matter voxels using the contrast "all stimulus conditions vs. the fixation baseline." In each ROI, we rank-ordered the resultant voxels by their t statistic (where $t > 0$) and selected to the top 300 voxels as data for the classification algorithm (Preston, Li, Kourtzi, & Welchman, 2008). To minimize baseline differences between runs we z-scored the response time course of each voxel and each experimental run. To account for the hemodynamic response lag, the fMRI time series were shifted by two repetition times (4 sec). Thereafter, we averaged the fMRI response of each voxel across the 16 sec stimulus presentation block, obtaining a single test pattern for the multivariate analysis per block. To remove potential univariate differences (that can be introduced after z-score normalization due to averaging across time points in a block and grouping the data into train vs. test data sets), we normalized by subtracting the mean of all voxels for a given volume (Serences & Boynton, 2007), with the result that each volume had the same mean value across voxels and differed only in the pattern of activity. We performed multivoxel pattern analysis using a linear support vector machine (SVM^light toolbox) classification algorithm. We trained the algorithm to distinguish between fMRI responses evoked by different stimulus configurations (e.g., convex to the left vs. to the right of fixation) for a given stimulus type (e.g., dis-

parity). Participants typically took part in eight runs, each of which had three repetitions of a given spatial configuration and stimulus type, creating a total of 24 patterns. We used a leave-one-run-out cross-validation procedure: We trained the classifier using seven runs (i.e., 21 patterns) and then evaluated the prediction performance of the classifier using the remaining, nontrained data (i.e., three patterns). We repeated this, leaving a single run out in turn, and calculated the mean prediction accuracy across cross-validation folds. Accuracies were represented in units of discriminability (d') using the formula:

$$d' = 2erfinv(2p-1) \tag{1}$$

where *erfinv* is the inverse error function and p is the proportion of correct predictions.

For tests of transfer between disparity and shading cues, we used a Recursive Feature Elimination method (De Martino et al., 2008) to detect sparse discriminative patterns and define the number of voxels for the SVM classification analysis. In each feature elimination step, five voxels were discarded until there remained a core set of voxels with the highest discriminative power. To avoid circular analysis, the Recursive Feature Elimination method was applied independently to the training patterns of each cross-validation fold, resulting in eight sets of voxels (i.e., one set for each test pattern of the leave-one-run-out procedure). This was done separately for each experimental condition, with final voxels for the SVM analysis chosen based on the intersection of voxels from corresponding cross-validation folds. A standard SVM was then used to compute within- and between-cue prediction accuracies. This feature selection method was required for transfer, in line with evidence that it improves generalization (De Martino et al., 2008).

We conducted repeated-measures GLM in SPSS (IBM, Inc., Armonk, NY) applying Greenhouse-Geisser correction when appropriate. Regression analyses were also conducted in SPSS. For this analysis, we considered the use of repeated-measures MANCOVA (and found results consistent with the regression results); however, the integration indices (defined below) we use are partially correlated between conditions because their calculation depends on the same denominator, violating the GLM's assumption of independence. We therefore limited our analysis to the relationship between psychophysical and fMRI indices for the same condition, for which the psychophysical and fMRI indices are independent of one another.

Quadratic Summation and Integration Indices

We formulate predictions for the combined cue condition (i.e., disparity + shading) based on the quadratic summation of performance in the component cue conditions (i.e., disparity, shading). As outlined in the Introduction, this prediction is based on the performance of
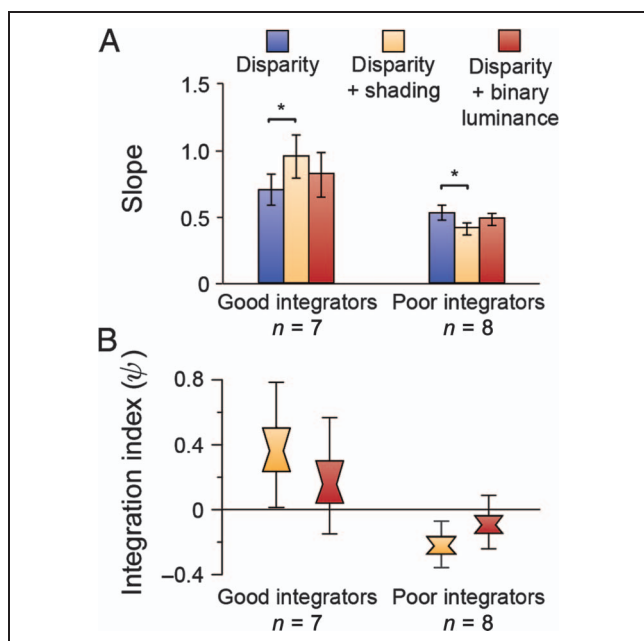
Figure 2. Psychophysical results. (A) Behavioral tests of integration. Bar graphs represent the between-subject mean slope of the psychometric function. *$p < .05$. (B) Psychophysical results as an integration index. Distribution plots show bootstrapped values: The center of the "bowtie" represents the median, the colored area depicts 68% confidence values, and the upper and lower error bars represent 95% confidence intervals.

an ideal observer model that discriminates pairs of inputs (visual stimuli or fMRI response patterns) based on the optimal discrimination boundary. Psychophysical tests indicate that this theoretical model matches human performance in combining cues (Knill & Saunders, 2003; Hillis, Ernst, Banks, & Landy, 2002).

To compare measured empirical performance in disparity + shading condition with the prediction derived from the component cue conditions, we calculate a ratio index (Ban et al., 2012; Nandy & Tjan, 2008) whose general form is

$$\text{Index} = \frac{C_{D+S}}{\sqrt{C_D^2 + C_S^2}} - 1 \qquad (2)$$

where C_D, C_S, and C_{D+S} are sensitivities for disparity, shading, and the combined cue conditions, respectively. If the responses of the detection mechanism to the disparity and shading conditions (C_D, C_S) are independent of each other, performance when both cues are available (C_{D+S}) should match the quadratic summation prediction, yielding a ratio of 1 and thus an index of zero. A value of less than zero suggests suboptimal detection performance, and a value above zero suggests that the component sources of information are not independent (Ban et al., 2012; Nandy & Tjan, 2008). However, a value above zero does not preclude the response of independent mechanisms: Depending on the amount of noise

introduced during fMRI measurement (scanner noise, observer movement), colocated but independent responses can yield a positive index (see the fMRI simulations by Ban et al., 2012 in their Supplementary Figure 3). Thus, the integration index alone cannot be taken as definite evidence of cue integration and therefore needs to be considered in conjunction with the other tests. To assess statistical significance of the integration indices, we used bootstrapped resampling as our use of a ratio makes distributions non-Normal, and thus a nonparametric procedure more appropriate.

RESULTS

Psychophysics

To assess cue integration psychophysically, we measured observers' sensitivity to slight differences in the depth profile of the stimuli (Figure 1B). Participants viewed two shapes sequentially, and decided which had the greater depth (i.e., which bumps were taller or which dimples were deeper). By comparing a given standard stimulus against a range of test stimuli, we obtained psychometric functions. We used the slope of these functions to quantify observers' sensitivity to stimulus differences (where a steeper slope indicates higher sensitivity). To determine whether there was a perceptual benefit associated with adding shading information to the stimuli, we compared performance in the disparity condition with that in the disparity and shading condition. Surprisingly, we found no evidence for enhanced performance in the disparity and shading condition at the group level, $F(1, 14) < 1$, $p = .38$. In light of previous empirical work on cue integration, this was unexpected (e.g., Lovell et al., 2012; Schiller et al., 2011; Vuong et al., 2006; Doorschot et al., 2001; Buelthoff & Mallot, 1988) and prompted us to consider the significant variability between observers, $F(1, 14) = 62.23$, $p < .001$, in their relative performance in the two conditions. In particular, we found that some participants clearly benefited from the presence of two cues; however, others showed no benefit and some actually performed worse relative to the disparity only condition. Poorer performance might relate to individual differences in the assumed direction of the illuminant (Schofield, Rock, & Georgeson, 2011); ambiguity or bistability in the interpretation of shading patterns (Wagemans, van Doorn, & Koenderink, 2010; Liu & Todd, 2004); and/or differences in cue weights (Lovell et al., 2012; Schiller et al., 2011; Knill & Saunders, 2003; we return to this issue in the Discussion). To quantify variations between participants in the relative performance in two conditions, we calculated a psychophysical integration index (ψ):

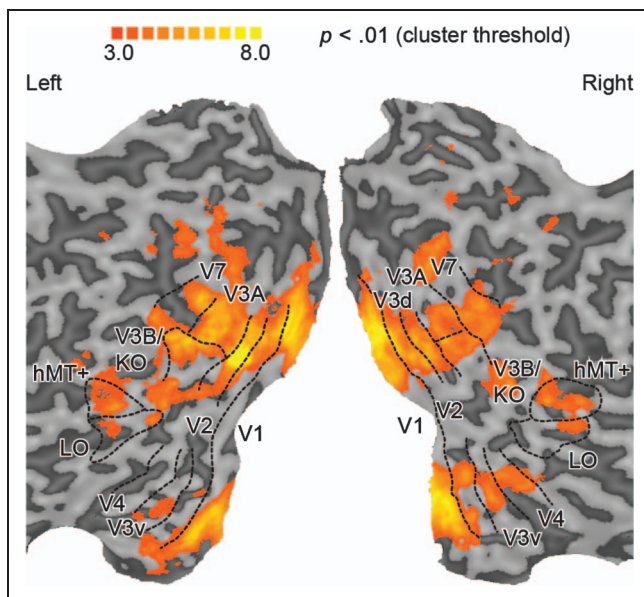$$\psi = \frac{S_{D+S}}{S_D} - 1 \qquad (3)$$

Figure 3. Representative flat maps from one participant showing the left and right ROIs. The sulci are depicted in darker gray than the gyri. Shown on the maps are retinotopic areas, V3B/KO, the human motion complex (hMT+/V5), and LO area. The activation on the maps shows the results of a searchlight classifier analysis that moved iteratively throughout the measured cortical volume, discriminating between stimulus configurations. The color code represents the *t* value of the classification accuracies obtained. This procedure confirmed that we had not missed any important areas outside those localized independently.

fMRI Measures

Before taking part in the main experiment, each participant underwent a separate fMRI session to identify ROIs within the visual cortex (Figure 3). We identified retinotopically organized cortical areas based on polar and eccentricity mapping techniques (Tyler et al., 2005; Tootell & Hadjikhani, 2001; DeYoe et al., 1996; Sereno et al., 1995). In addition, we identified area LO involved in object processing (Kourtzi & Kanwisher, 2001), the human motion complex (hMT[+]/V5; Zeki et al., 1991), and the KO region, which is localized by contrasting motion-defined contours with transparent motion (Zeki et al., 2003; Dupont et al., 1997). Responses to the KO localizer overlapped with the retinotopically localized area V3B and were not consistently separable across participants and/or hemispheres (see also Ban et al., 2012) so we denote this region as V3B/KO. A representative flatmap of the ROIs is shown in Figure 3, and Table 1 provides mean coordinates for V3B/KO.

We then measured fMRI responses in each of the ROIs and were a priori particularly interested in the V3B/KO region (Ban et al., 2012; Tyler, Likova, Kontsevich, & Wade, 2006). We presented stimuli from four experimental conditions (Figure 1) under two configurations: (a) bumps to the left of fixation, dimples to the right or (b) bumps to the right, dimples to the left, thereby allowing us to contrast fMRI responses to convex versus concave stimuli.

To analyze our data, we trained a machine learning classifier (SVM) to associate patterns of fMRI voxel activity and the stimulus configuration (convex vs. concave) that gave rise to that activity. We used the performance of the
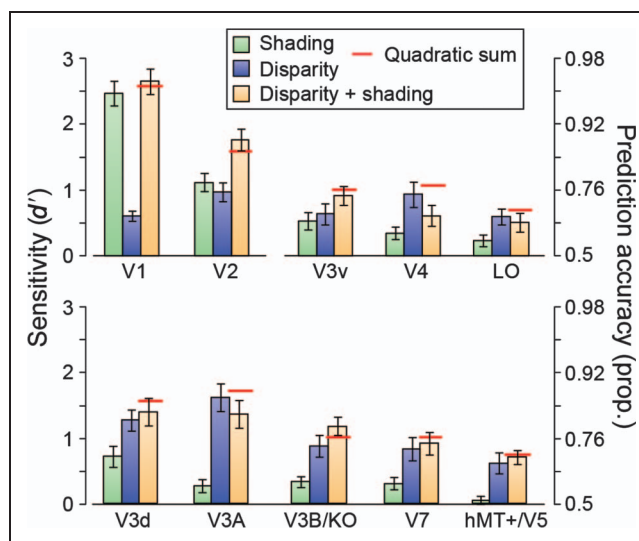
where S_{D+S} is sensitivity in the combined condition and S_D is sensitivity in the disparity condition. This index is based on the quadratic summation test (Ban et al., 2012; Nandy & Tjan, 2008; see Methods) where a value above zero suggests that participants integrate the depth information provided by the disparity and shading cues when making perceptual judgments. In this instance we assumed that $S_D \approx \sqrt{(S_D^2 + S_S^2)}$ because our attempts to measure sensitivity to differences in depth amplitude defined by shading alone in pilot testing resulted in such poor performance that we could not fit a reliable psychometric function. Specifically, discriminability for the maximum presented depth difference was $d' = 0.3 \pm 0.25$ for shading alone, in contrast to $d' = 3.9 \pm 0.3$ for disparity, that is, $S_D^2 \gg S_S^2$.

We used a clustering algorithm on ψ to determine whether our participants formed different subgroups. In particular, SPSS's two-step clustering algorithm (applying Schwarz's Bayesian Criterion for cluster identification) indicated two subgroups: Participants with $\psi > 0.1$ were associated with cluster 1 and participants with $\psi < -0.1$ with cluster 2; hereafter, we refer to these groups as *good integrators* (*n* = 7) and *poor integrators* (*n* = 8). By definition, these post hoc groups differed in the relative sensitivity to disparity and disparity + shading conditions (Figure 2). Our purpose in forming these groups, however, was to test the link between differences in perception and fMRI responses.

Figure 4. Performance in predicting the convex versus concave configuration of the stimuli based on the fMRI data measured in different ROIs. The bar graphs show the results from the "single cue" experimental conditions, the "disparity + shading" condition, and the quadratic summation prediction (horizontal red line). Error bars indicate *SEM*.

classifier in decoding the stimulus from independent fMRI data (i.e., leave-one-run-out cross validation) as a measure of the information about the presented stimulus within a particular region of cortex.

We could reliably decode the stimulus configuration in the four conditions in almost every ROI (Figure 4), and there was a clear interaction between conditions and ROIs, $F(8.0, 104.2) = 8.92$, $p < .001$. This widespread sensitivity to differences between convex versus concave stimuli is not surprising in that a range of features might modify the fMRI response (e.g., distribution of image intensities, contrast edges, mean disparity, etc.). The machine learning classifier may thus decode low-level image features, rather than "depth" per se. We were therefore interested not in overall prediction accuracies between areas (which are influenced by our ability to measure fMRI activity in different anatomical locations). Rather, we were interested in the relative performance between conditions, and whether this related to between-observer differences in perceptual integration. We therefore considered our fMRI data subdivided based on the behavioral results (significant interaction between condition and group [good vs. poor integrators]: $F(2.0, 26.6) = 4.52$, $p = .02$).

First, we wished to determine whether fMRI decoding performance improved when both depth cues indicated depth differences. Prediction accuracies for the concurrent stimulus (disparity + shading) were statistically higher than the component cues in areas V2, $F(3, 39) = 7.47$, $p < .001$, and V3B/KO, $F(1.6, 21.7) = 14.88$, $p < .001$. To assess integration, we compared the extent of improvement in the concurrent stimulus relative to a minimum bound prediction (Figures 4 and 5, red lines) based on the quadratic summation of decoding accuracies for

"single cue" presentations (Ban et al., 2012). This corresponds to the level of performance expected if disparity signals and shading signals are collocated in a cortical area, but represented independently. If performance exceeds this bound, it suggests that cue representations are not independent, as performance in the "single" cue case was attenuated by the conflicts that result from "isolating" the cue. We found that performance was higher (outside the *SEM*) than the quadratic summation prediction in areas V2 and V3B/KO (Figure 5). However, this result was only statistically reliable in V3B/KO. Specifically in V3B/KO, there was a significant interaction between the behavioral group and experimental condition, $F(2, 26) = 5.52$, $p = .01$, with decoding performance in the concurrent (disparity + shading) condition exceeding the quadratic summation prediction for good integrators, $F(1, 6) = 9.27$, $p = .011$, but not for the poor integrators, $F(1, 7) < 1$, $p = .35$ (Figure 5). In V2, there was no significant difference between the quadratic summation prediction and the measured data in the combined cue conditions, $F(2, 26) < 1$, $p = .62$, nor an interaction, $F(2, 26) = 2.63$, $p = .091$. We quantified the extent of integration using a bootstrapped index (ϕ) that contrasted decoding performance in the concurrent condition (d'_{D+S}) with the quadratic summation of performance with "single" cues (d'_D and d'_S):

$$\phi = \frac{d'_{D+S}}{\sqrt{d'_D{}^2 + d'_S{}^2}} - 1 \qquad (4)$$

Using this index, a value of zero corresponds to the performance expected if information from disparity
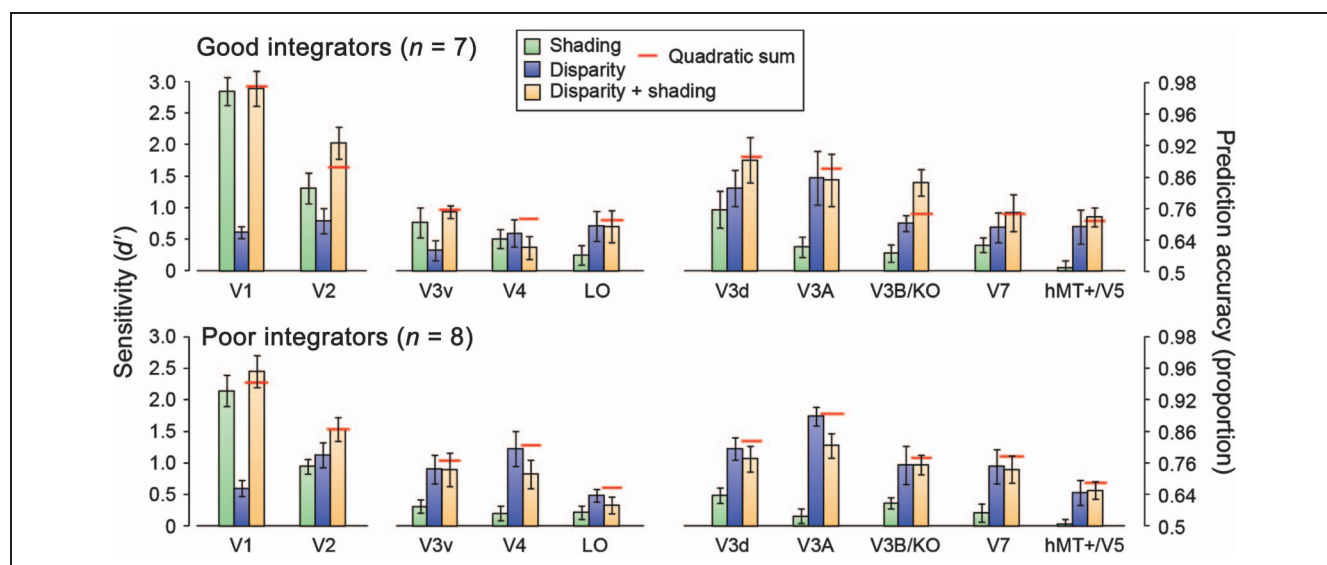

Figure 5. Prediction performance for fMRI data separated into the two groups based on the psychophysical results ("good" vs. "poor" integrators). The bar graphs show the results from the "single cue" experimental conditions, the "disparity + shading" condition, and the quadratic summation prediction (horizontal red line). Error bars indicate *SEM*.
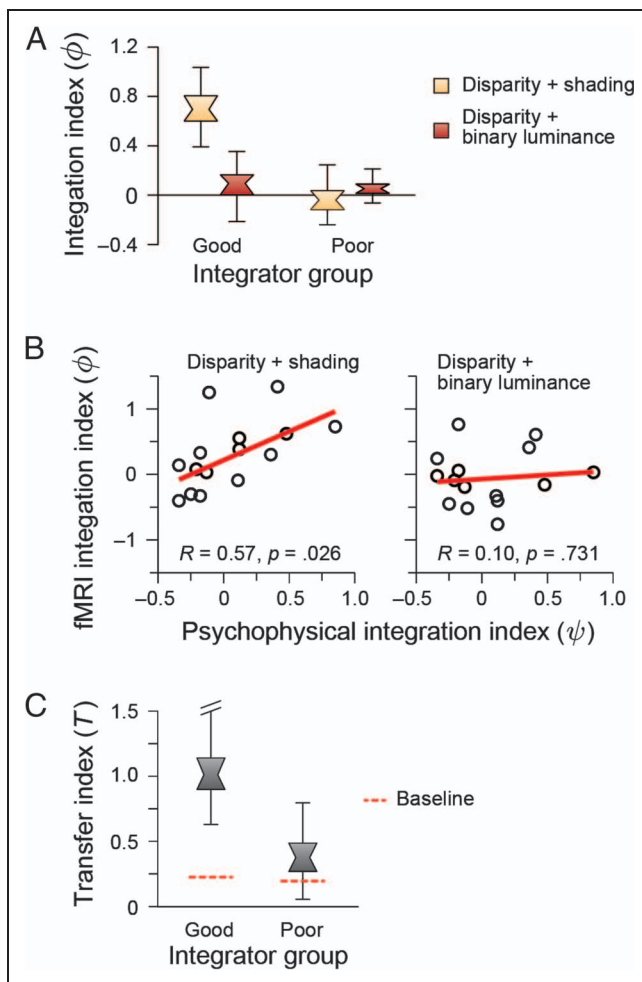
Figure 6. (A) fMRI based prediction performance as an integration index for the two groups of participants in area V3B/KO. A value of zero indicates the minimum bound for fusion as predicted by quadratic summation. The index is calculated for the "disparity + shading" and "disparity + binary shading" conditions. Data are presented as notched distribution plots. The center of the "bowtie" represents the median, the colored area depicts 68% confidence values, and the upper and lower error bars represent 95% confidence intervals. (B) Correlation between behavioral and fMRI integration indices in area V3B/KO. Psychophysics and fMRI integration indices are plotted for each participant for disparity + shading and disparity + binary luminance conditions. The Pearson correlation coefficient (R) and *p* value are shown. (C) The transfer index values for V3B/KO for the good and poor integrator groups. Using this index, a value of 1 indicates equivalent prediction accuracies when training and testing on the same cue versus training and testing on different cues. Distribution plots show the median, 68% and 95% confidence intervals. Dotted horizontal lines depict a bootstrapped chance baseline based on the upper 95th centile for transfer analysis obtained with randomly permuted data.

and shading are collocated, but independent. We found that only in areas V2 and V3B/KO was the integration index for the concurrent condition reliably above zero for the good integrators (Figure 6A; Table 2).

To provide additional evidence for neuronal responses related to depth estimation, we used the binary luminance stimuli as a control. We constructed these stimuli such that they contained a very obvious low-level feature

that approximated luminance differences in the shaded stimuli but did not, per se, evoke an impression of depth. As the fMRI response in a given area may reflect low-level stimulus differences (rather than depth from shading), we wanted to rule out the possibility that improved decoding performance in the concurrent disparity + shading condition could be explained on the basis that two separate stimulus dimensions (disparity and luminance) drive the fMRI response. The quadratic summation test should theoretically rule this out; nevertheless, we contrasted decoding performance in the concurrent condition versus the binary control (disparity + binary luminance) condition. We reasoned that if enhanced decoding is related to the representation of depth, superquadratic summation effects would be limited to the concurrent condition. On the basis of a significant interaction between subject group and condition, $F_{(2, 26)} = 5.52$, $p = .01$, we found that this was true for the good integrator subjects in area V3B/KO: sensitivity in the concurrent condition was above that in the binary control condition, $F_{(1, 6)} = 14.69$, $p = .004$. By contrast, sensitivity for the binary condition in the poor integrator subjects matched that of the concurrent group, $F_{(1, 7)} < 1$, $p = .31$, and was in line with quadratic summation. Results from other ROIs (Table 2) did not suggest the clear (or significant) differences that were apparent in V3B/KO.

As a further line of evidence, we used regression analyses to test the relationship between psychophysical and fMRI measures of integration. Although we would not anticipate a one-to-one mapping between them (the fMRI data were obtained for differences between concave vs. convex shapes, whereas the psychophysical tests measured sensitivity to slight differences in the depth profile), our group-based analysis suggested a correspondence. We found a significant relationship between the fMRI and psychophysical integration indices in V3B/KO (Figure 6B) for the concurrent ($R = 0.57$, $p = .026$) but not the binary luminance ($R = 0.10$, $p = .731$) condition. This result was specific to area V3B/KO (Table 3) and, in line with the preceding analyses, suggests a relationship between activity in area V3B/KO and the perceptual integration of disparity and shading cues to depth.

As a final assessment of whether fMRI responses related to depth structure from different cues, we tested whether training the classifier on depth configurations from one cue (e.g., shading) afforded predictions for depth configurations specified by the other (e.g., disparity). To compare the prediction accuracies on this cross-cue transfer with baseline performance (i.e., training and testing on the same cue), we used a bootstrapped transfer index:

$$T = \frac{2d'_{\mathrm{T}}}{d'_{\mathrm{D}} + d'_{\mathrm{S}}} \qquad (5)$$

where d'_{T} is between-cue transfer performance and ½ ($d'_{\mathrm{D}} + d'_{\mathrm{S}}$) is the average within-cue performance. A

Table 2. Probabilities Associated with Obtaining a Value of Zero for the fMRI Integration Index in the (i) Disparity + Shading Condition and (ii) Luminance Control Condition

Cortical Area	Disparity + Shading		Disparity + Binary Luminance	
	Good Integrators	Poor Integrators	Good Integrators	Poor Integrators
V1	0.538	0.157	0.999	0.543
V2	**0.004**	0.419	0.607	0.102
V3v	0.294	0.579	0.726	1.000
V4	0.916	0.942	0.987	0.628
LO	0.656	0.944	0.984	0.143
V3d	0.253	0.890	0.909	0.234
V3A	0.609	1.000	0.999	0.961
V3B/KO	**<0.001**	0.629	0.327	0.271
V7	0.298	0.595	0.844	0.620
hMT$^+$/V5	0.315	0.421	0.978	0.575

Values are from a bootstrapped resampling of the individual participants' data using 10,000 samples. **Bold** formatting indicates Bonferroni-corrected significance.

value of one using this index indicates that prediction accuracy between cues equals that within cues. To provide a baseline for the transfer that might occur by chance, we calculated the transfer index on data sets for which we randomly shuffled the condition labels, such that we broke the relationship between fMRI response and the stimulus that evoked the response. We calculated shuffled transfer performance 1000 times for each ROI and used the 95th centile of the resulting distribution of transfer indices as the

Table 3. Results for the Regression Analyses Relating the Psychophysical and fMRI Integration Indices in Each ROI

Cortical Area	Disparity + Shading		Disparity + Binary Luminance	
	R	p	R	p
V1	−0.418	.121	−0.265	.340
V2	0.105	.709	−0.394	.146
V3v	−0.078	.782	0.421	.118
V4	0.089	.754	−0.154	.584
LO	0.245	.379	−0.281	.311
V3d	0.194	.487	−0.157	.577
V3A	0.232	.405	−0.157	.577
V3B/KO	**0.571**	**.026**	0.097	.731
V7	0.019	.946	−0.055	.847
hMT$^+$/V5	0.411	.128	−0.367	.178

The table shows the Pearson correlation coefficient (R) and the significance of the fit as a p value for the "disparity + shading" and "disparity + binary luminance" conditions.

cut-off for significance. We found reliable evidence for transfer between cues in area V3B/KO (Figure 6C) for the good, but not poor, integrator groups. Furthermore, this effect was specific to V3B/KO and was not observed in other areas (Table 4). Together with the previous analyses, this result suggests a degree of equivalence between representations of depth from different cues in V3B/KO that is related to an individual's perceptual interpretation of cues.

To ensure we had not missed any important loci of activity outside the areas we sampled using our ROI localizers, we conducted a searchlight classification analysis (Kriegeskorte, Goebel, & Bandettini, 2006) in which we moved a small spherical aperture (diameter = 9 mm) through the sampled cortical volume performing MVPA on the difference between stimulus configurations for the concurrent cue condition (Figure 3). This analysis indicated that discriminative signals about stimulus differences were well captured by our ROI definitions.

Our main analyses considered MVPA of the fMRI responses partitioned into two groups based on psychophysical performance. To ensure that differences in MVPA prediction performance between groups related to the pattern of voxel responses for depth processing, rather than the overall responsiveness of different ROIs, we calculated the average fMRI activations (percent signal change) in each ROI for the two groups of participants. Reassuringly, we found no evidence for statistically reliable differences between groups across conditions and ROIs (i.e., no ROI × Group interaction: $F(3.3, 43.4) < 1$, $p = .637$; no Condition × Group interaction: $F(3.5, 45.4) < 1$, $p = .902$; and no ROI × Condition × Group interaction: $F(8.6, 112.2) = 1.06$, $p = .397$). Moreover, limiting this analysis to V3B/KO provided no evidence

Table 4. Probabilities Associated with the Transfer between Disparity and Shading Producing a Transfer Index above the Random (Shuffled) Baseline

Cortical Area	Good Integrators	Poor Integrators
V1	0.247	0.748
V2	0.788	0.709
V3v	0.121	0.908
V4	0.478	0.062
LO	0.254	0.033
V3d	0.098	0.227
V3A	0.295	0.275
V3B/KO	**<0.001**	0.212
V7	0.145	0.538
hMT$^+$/V5	0.124	0.302

These p values are calculated using bootstrapped resampling with 10,000 samples. **Bold** formatting indicates Bonferroni-corrected significance.

for a difference in the percent signal change between groups (i.e., no Condition × Group interaction: $F(3.1, 40.3) < 1$, $p = .586$). Furthermore, we ensured that we had sampled from the same cortical location in both groups by calculating the mean Talairach location of V3B/KO subdivided by groups (Table 1). This confirmed that we had localized the same cortical region in both groups of participants.

To guard against artifacts complicating the interpretation of our results, we took specific precautions during scanning to control attentional allocation and eye movements. First, participants performed a demanding vernier judgment task at fixation. This ensured equivalent attentional allocation across conditions, and, as the task was unrelated to the depth stimuli, psychophysical judgments and fMRI responses were not confounded and could not thereby explain between-subject differences. Second, the attentional task served to provide a subjective measure of eye vergence (Popple et al., 1998). In particular, participants judged the relative location of a small target flashed (250 msec) to one eye, relative to the upper vertical nonius line (presented to the other eye; Figure 1D). We fit the proportion of "target is to the right" responses as a function of the target's horizontal displacement. Bias (i.e., deviation from the desired vergence position) in this judgment was around zero suggesting that participants were able to maintain fixation with the required vergence angle. Using a repeated-measures ANOVA, we found that there were no significant differences in bias between Stimulus Conditions, $F(1.5, 21.4) = 2.59$, $p = .109$, Sign of Curvature, $F(1, 14) = 1.43$, $p = .25$, and no interaction, $F(2.2, 30.7) = 1.95$, $p = .157$. Furthermore, there were no differences in the slope of the psychometric functions: no effect of Condition, $F(3, 42) < 1$, $p = .82$, or Curvature,

$F(1, 14) < 1$, $p = .80$, and no interaction, $F(3, 42) < 1$, $p = .85$.

Third, our stimuli were constructed to reduce the potential for vergence differences: Disparities to the left and right of the fixation point were equal and opposite, a constant low spatial frequency pattern surrounded the stimuli, and participants used horizontal and vertical nonius lines to monitor their eye vergence.

DISCUSSION

Here we provide three lines of evidence that activity in dorsal visual area V3B/KO reflects the integration of disparity and shading depth cues in a perceptually relevant manner. First, we used a quadratic summation test to show that performance in concurrent cue settings improves beyond that expected if depth from disparity and shading are collocated but represented independently. Second, we showed that this result was specific to stimuli that are compatible with a 3-D interpretation of shading patterns. Third, we found evidence for cross-cue transfer. Importantly, the strength of these results in V3B/KO varied between individuals in a manner that was compatible with their perceptual use of integrated depth signals.

These findings complement evidence for the integration of disparity and relative motion in area V3B/KO (Ban et al., 2012) and suggest both a strong link with perceptual judgments and a more generalized representation of depth structure. Such generalization is far from trivial: Binocular disparity is a function of an object's 3-D structure, its distance from the viewer and the separation between the viewer's eyes; by contrast, shading cues (i.e., intensity distributions in the image) depend on the type of illumination, the orientation of the light source with respect to the 3-D object, and the reflective properties of the object's surface (i.e., the degree of Lambertian and Specular reflectance). As such disparity and shading provide complementary shape information: They have quite different generative processes, and their interpretation depends on different constraints and assumptions (Doorschot et al., 2001; Blake, Zisserman, & Knowles, 1985). Taken together, these results indicate that the 3-D representations in the V3B/KO region are not specific to specific cue pairs (i.e., disparity–motion) and generalize to more complex forms of 3-D structural information (i.e., local curvature). This points to an important role for higher portions of the dorsal visual cortex in computing information about the 3-D structure of the surrounding environment.

Individual Differences in Disparity and Shading Integration

One striking, and unexpected feature of our findings was that we observed significant between-subject variability in the extent to which shading enhanced performance, with

some participants benefitting, and others actually performing worse. What might be responsible for this variation in performance? Although shading cues support reliable judgments of ordinal structure (Ramachandran, 1988), shape is often underestimated (Mingolla & Todd, 1986) and subject to systematic biases related to the estimated light source position (Mamassian & Goutcher, 2001; Sun & Perona, 1998; Curran & Johnston, 1996; Pentland, 1982) and light source composition (Schofield et al., 2011). Moreover, assumptions about the position of the light source in the scene are often esoteric: Most observers assume overhead lighting, but the strength of this assumption varies considerably (Thomas, Nardini, & Mareschal, 2010; Wagemans et al., 2010; Liu & Todd, 2004), and some observers assume lighting from below (e.g., 3 of 15 participants in Schofield et al., 2011). Our disparity + shading stimuli were designed such that the cues indicated the same depth structure to an observer who assumed lighting from above. Therefore, it is quite possible that observers experienced conflict between the shape information specified by disparity and that determined by their interpretation of the shading pattern. Such participants would be "poor integrators" only inasmuch as they failed to share the assumptions typically made by observers (i.e., lighting direction, lighting composition, and Lambertian surface reflectance) when interpreting shading patterns. In addition, participants may have experienced alternation in their interpretation of the shading cue across trials (i.e., a weak light-from-above assumption that has been observed quite frequently; Thomas et al., 2010; Wagemans et al., 2010); aggregating such bimodal responses to characterize the psychometric function would result in more variable responses in the concurrent condition than in the "disparity" alone condition, which was not subject to perceptual bistability. Such variations could also result in fMRI responses that vary between trials; in particular, fMRI responses in V3B/KO change in line with different perceptual interpretations of the same (ambiguous) 3-D structure indicated by shading cues (Preston, Kourtzi, & Welchman, 2009). This variation in fMRI responses could thereby account for reduced decoding performance for these participants.

An alternative possibility is that some of our observers did not integrate information from disparity and shading because they are inherently poor integrators. Although cue integration both within and between sensory modalities has been widely reported in adults, it has a developmental trajectory and young children do not integrate signals (Gori, Del Viva, Sandini, & Burr, 2008; Nardini, Jones, Bedford, & Braddick, 2008; Nardini, Bedford, & Mareschal, 2010). This suggests that cue integration may be learnt via exposure to correlated cues (Atkins, Fiser, & Jacobs, 2001) where the effectiveness of learning can differ between observers (Ernst, 2007). Furthermore, although cue integration may be mandatory for many cues where such correlations are prevalent (Hillis et al., 2002), interindividual variability in the prior assumptions

that are used to interpret shading patterns may cause some participants to lack experience of integrating shading and disparity cues (at least in terms of how these are studied in the laboratory).

These different possibilities are difficult to distinguish from previous work that has looked at the integration of disparity and shading signals and reported individual results. This work indicated that perceptual judgments are enhanced by the combination of disparity and shading cues (Lovell et al., 2012; Schiller et al., 2011; Vuong et al., 2006; Doorschot et al., 2001; Buelthoff & Mallot, 1988). However, between-participant variation in such enhancement is difficult to assess given that low numbers of participants were used (mean per study = 3.6, max = 5), a sizeable proportion of whom were not naive to the purposes of the study. Here we find evidence for integration in both authors H.B. and A.W., but considerable variability among the naive participants. In common with Wagemans et al. (2010), this suggests that interobserver variability may be significant in the interpretation of shading patterns in particular and integration more generally, providing a stimulus for future work to explain the basis for such differences.

Responses in Other ROIs

When presenting the results for all the participants, we noted that performance in the disparity + shading condition was statistically higher than for the component cues in area V2 as well as in V3B/KO (Figure 3). Our subsequent analyses did not provide evidence that V2 is a likely substrate for the integration of disparity and shading cues. However, it is possible that the increased decoding performance—around the level expected by quadratic summation—is due to parallel representations of disparity and shading information. It is unlikely that either signal is fully elaborated, but V2's more spatially extensive receptive fields may provide important information about luminance and contrast variations across the scene that provide signals important when interpreting shape from shading (Schofield et al., 2010).

Previous work (Georgieva et al., 2008) suggested that the processing of 3-D structure from shading is primarily restricted in its representation to a ventral locus near the area we localize as LO (although Gerardin, Kourtzi, & Mamassian, 2010 suggested V3B/KO is also involved and Taira, Nose, Inoue, & Tsutsui, 2001 reported widespread responses). Our fMRI data supported only weak decoding of depth configurations defined by shading in LO, and more generally across higher portions of both the dorsal and ventral visual streams (Figures 3 and 4). Indeed, the highest prediction performance of the MVPA classifier for shading (relative to overall decoding accuracies in each ROI) was observed in V1 and V2, which is likely to reflect low-level image differences between stimulus configurations rather than an estimate of shape from shading per se. Nevertheless, our findings from V3B/KO

make it clear that information provided by shading contributes to fMRI responses in higher portions of the dorsal stream. Why then is performance in the "shading" condition so low? Our experimental stimuli purposefully provoked conflicts between the disparity and shading information in the "single cue" conditions. Therefore, the conflicting information from disparity that the viewed surface was flat is likely to have attenuated fMRI responses to the "shading alone" stimulus. Indeed, given that sensitivity to disparity differences was so much greater than for shading, it might appear surprising that we could decode shading information at all. Previously, we used mathematical simulations to suggest that area V3B/KO contains a mixed population of responses, with some units responding to individual cues and others fusing cues into a single representation (Ban et al., 2012). Thus, residual fMRI decoding performance for the shading condition may reflect responses to nonintegrated processing of the shading aspects of the stimuli. This mixed population could help support a robust perceptual interpretation of stimuli that contain significant cue conflicts: for example, the reader should still be able to gain an impression of the 3-D structure of the shaded stimuli in Figure 1, despite conflicts with disparity).

In summary, previous fMRI studies suggest a number of locations in which 3-D shape information might be processed (Nelissen et al., 2009; Sereno et al., 2002). Here we provide evidence that area V3B/KO plays an important role in integrating disparity and shading cues, compatible with the notion that it represents 3-D structure from different signals (Tyler et al., 2006) that are subject to different prior constraints (Preston et al., 2009). Our results suggest that V3B/KO is involved in 3-D estimation from qualitatively different depth cues, and its activity may underlie perceptual judgments of depth.

Acknowledgments

REFERENCES

Anzai, A., Ohzawa, I., & Freeman, R. D. (2001). Joint-encoding of motion and depth by visual cortical neurons: Neural basis of the Pulfrich effect. *Nature Neuroscience, 4,* 513–518.

Atkins, J. E., Fiser, J., & Jacobs, R. A. (2001). Experience-dependent visual cue integration based on consistencies between visual and haptic percepts. *Vision Research, 41,* 449–461.

Ban, H., Preston, T. J., Meeson, A., & Welchman, A. E. (2012). The integration of motion and disparity cues to depth in dorsal visual cortex. *Nature Neuroscience, 15,* 636–643.

Belhumeur, P. N., Kriegman, D. J., & Yuille, A. L. (1999). The bas-relief ambiguity. *International Journal of Computer Vision, 35,* 33–44.

Blake, A., Zisserman, A., & Knowles, G. (1985). Surface descriptions from stereo and shading. *Image and Vision Computing, 3,* 183–191.

Bradley, D. C., Qian, N., & Andersen, R. A. (1995). Integration of motion and stereopsis in middle temporal cortical area of macaques. *Nature, 373,* 609–611.

Buelthoff, H. H., & Mallot, H. A. (1988). Integration of depth modules - Stereo and shading. *Journal of the Optical Society of America: A, 5,* 1749–1758.

Burge, J., Fowlkes, C. C., & Banks, M. S. (2010). Natural-scene statistics predict how the figure-ground cue of convexity affects human depth perception. *Journal of Neuroscience, 30,* 7269–7280.

Curran, W., & Johnston, A. (1996). The effect of illuminant position on perceived curvature. *Vision Research, 36,* 1399–1410.

De Martino, F., Valente, G., Staeren, N., Ashburner, J., Goebel, R., & Formisano, E. (2008). Combining multivariate voxel selection and support vector machines for mapping and classification of fMRI spatial patterns. *Neuroimage, 43,* 44–58.

DeAngelis, G. C., & Uka, T. (2003). Coding of horizontal disparity and velocity by MT neurons in the alert macaque. *Journal of Neurophysiology, 89,* 1094–1111.

DeYoe, E. A., Carman, G. J., Bandettini, P., Glickman, S., Wieser, J., Cox, R., et al. (1996). Mapping striate and extrastriate visual areas in human cerebral cortex. *Proceedings of the National Academy of Sciences, U.S.A., 93,* 2382–2386.

Doorschot, P. C. A., Kappers, A. M. L., & Koenderink, J. J. (2001). The combined influence of binocular disparity and shading on pictorial shape. *Perception & Psychophysics, 63,* 1038–1047.

Dosher, B. A., Sperling, G., & Wurst, S. A. (1986). Tradeoffs between stereopsis and proximity luminance covariance as determinants of perceived 3-D structure. *Vision Research, 26,* 973–990.

Dupont, P., De Bruyn, B., Vandenberghe, R., Rosier, A. M., Michiels, J., Marchal, G., et al. (1997). The kinetic occipital region in human visual cortex. *Cerebral Cortex, 7,* 283–292.

Ernst, M. O. (2007). Learning to integrate arbitrary signals from vision and touch. *Journal of Vision, 7,* 1–14.

Fleming, R. W., Dror, R. O., & Adelson, E. H. (2003). Real-world illumination and the perception of surface reflectance properties. *Journal of Vision, 3,* 347–368.

Georgieva, S. S., Todd, J. T., Peeters, R., & Orban, G. A. (2008). The extraction of 3-D shape from texture and shading in the human brain. *Cerebral Cortex, 18,* 2416–2438.

Gerardin, P., Kourtzi, Z., & Mamassian, P. (2010). Prior knowledge of illumination for 3-D perception in the human brain. *Proceedings of the National Academy of Sciences, U.S.A., 107,* 16309–16314.

Gori, M., Del Viva, M., Sandini, G., & Burr, D. C. (2008). Young children do not integrate visual and haptic form information. *Current Biology, 18,* 694–698.

Grill-Spector, K., Kushnir, T., Hendler, T., & Malach, R. (2000). The dynamics of object-selective activation correlate with recognition performance in humans. *Nature Neuroscience, 3,* 837–843.

Hillis, J. M., Ernst, M. O., Banks, M. S., & Landy, M. S. (2002). Combining sensory information: Mandatory fusion within, but not between, senses. *Science, 298,* 1627–1630.

Horn, B. K. P. (1975). Obtaining shape from shading information. In P. H. Winston (Ed.), *The psychology of computer vision* (pp. 115–155). New York: McGraw Hill.

Janssen, P., Vogels, R., & Orban, G. A. (2000). Three-dimensional shape coding in inferior temporal cortex. *Neuron, 27,* 385–397.

Kersten, D., Mamassian, P., & Yuille, A. (2004). Object perception as Bayesian inference. *Annual Review of Psychology, 55,* 271–304.

Kingdom, F. A. A. (2003). Color brings relief to human vision. *Nature Neuroscience, 6,* 641–644.

Knill, D. C., & Saunders, J. A. (2003). Do humans optimally integrate stereo and texture information for judgments of surface slant? *Vision Research, 43,* 2539–2558.

Koenderink, J. J., & van Doorn, A. J. (2003). Shape and shading. In L. M. Chalupa & J. S. Werner (Eds.), *The visual neurosciences* (pp. 1090–1105). Cambridge, MA: MIT Press.

Kourtzi, Z., & Kanwisher, N. (2001). Representation of perceived object shape by the human lateral occipital complex. *Science, 293,* 1506–1509.

Kriegeskorte, N., Goebel, R., & Bandettini, P. (2006). Information-based functional brain mapping. *Proceedings of the National Academy of Sciences, U.S.A., 103,* 3863–3868.

Landy, M. S., Maloney, L. T., Johnston, E. B., & Young, M. (1995). Measurement and modeling of depth cue combination - In defense of weak fusion. *Vision Research, 35,* 389–412.

Larsson, J., Heeger, D. J., & Landy, M. S. (2010). Orientation selectivity of motion-boundary responses in human visual cortex. *Journal of Neurophysiology, 104,* 2940–2950.

Lee, Y. L., & Saunders, J. A. (2011). Stereo improves 3-D shape discrimination even when rich monocular shape cues are available. *Journal of Vision, 11,* Article 2.

Liu, B., & Todd, J. T. (2004). Perceptual biases in the interpretation of 3-D shape from shading. *Vision Research, 44,* 2135–2145.

Lovell, P. G., Bloj, M., & Harris, J. M. (2012). Optimal integration of shading and binocular disparity for depth perception. *Journal of Vision, 12,* 1–18.

Mamassian, P., & Goutcher, R. (2001). Prior knowledge on the illumination position. *Cognition, 81,* B1–B9.

Mingolla, E., & Todd, J. T. (1986). Perception of solid shape from shading. *Biological Cybernetics, 53,* 137–151.

Nandy, A. S., & Tjan, B. S. (2008). Efficient integration across spatial frequencies for letter identification in foveal and peripheral vision. *Journal of Vision, 8,* 1–20.

Nardini, M., Bedford, R., & Mareschal, D. (2010). Fusion of visual cues is not mandatory in children. *Proceedings of the National Academy of Sciences, U.S.A., 107,* 17041–17046.

Nardini, M., Jones, P., Bedford, R., & Braddick, O. (2008). Development of cue integration in human navigation. *Current Biology, 18,* 689–693.

Nelissen, K., Joly, O., Durand, J. B., Todd, J. T., Vanduffel, W., & Orban, G. A. (2009). The extraction of depth structure from shading and texture in the macaque brain. *Plos One, 4,* e8306.

Pentland, A. P. (1982). Finding the illuminant direction. *Journal of the Optical Society of America, 72,* 448–455.

Popple, A. V., Smallman, H. S., & Findlay, J. M. (1998). The area of spatial integration for initial horizontal disparity vergence. *Vision Research, 38,* 319–326.

Preston, T. J., Kourtzi, Z., & Welchman, A. E. (2009). Adaptive estimation of three-dimensional structure in the human brain. *Journal of Neuroscience, 29,* 1688–1698.

Preston, T. J., Li, S., Kourtzi, Z., & Welchman, A. E. (2008). Multivoxel pattern selectivity for perceptually relevant binocular disparities in the human brain. *Journal of Neuroscience, 28,* 11315–11327.

Ramachandran, V. S. (1988). Perception of shape from shading. *Nature, 331,* 163–166.

Richards, W. (1985). Structure from stereo and motion. *Journal of the Optical Society of America: A, 2,* 343–349.

Schiller, P. H., Slocum, W. M., Jao, B., & Weiner, V. S. (2011). The integration of disparity, shading and motion parallax cues for depth perception in humans and monkeys. *Brain Research, 1377,* 67–77.

Schofield, A. J., Rock, P. B., & Georgeson, M. A. (2011). Sun and sky: Does human vision assume a mixture of point and diffuse illumination when interpreting shape-from-shading? *Vision Research, 51,* 2317–2330.

Schofield, A. J., Rock, P. B., Sun, P., Jiang, X. Y., & Georgeson, M. A. (2010). What is second-order vision for? Discriminating illumination versus material changes. *Journal of Vision, 10.*

Serences, J. T., & Boynton, G. M. (2007). The representation of behavioral choice for motion in human visual cortex. *Journal of Neuroscience, 27,* 12893–12899.

Sereno, M. E., Trinath, T., Augath, M., & Logothetis, N. K. (2002). Three-dimensional shape representation in monkey cortex. *Neuron, 33,* 635–652.

Sereno, M. I., Dale, A. M., Reppas, J. B., Kwong, K. K., Belliveau, J. W., Brady, T. J., et al. (1995). Borders of multiple visual areas in humans revealed by functional magnetic resonance imaging. *Science, 268,* 889–893.

Srivastava, S., Orban, G. A., De Maziere, P. A., & Janssen, P. (2009). A distinct representation of three-dimensional shape in macaque anterior intraparietal area: Fast, metric, and coarse. *Journal of Neuroscience, 29,* 10613–10626.

Sun, J., & Perona, P. (1998). Where is the sun? *Nature Neuroscience, 1,* 183–184.

Taira, M., Nose, I., Inoue, K., & Tsutsui, K. (2001). Cortical areas related to attention to 3-D surface structures based on shading: An fMRI study. *Neuroimage, 14,* 959–966.

Thomas, R., Nardini, M., & Mareschal, D. (2010). Interactions between "light-from-above" and convexity priors in visual development. *Journal of Vision, 10,* 6.

Thompson, W. B., Fleming, R. W., Creem-Regehr, S. H., & Stefanucci, J. K. (2011). Illumination, shading and shadows. *Chapter 9 of Visual perception from a computer graphics perspective.* Boca Raton, FL: Taylor and Francis.

Tootell, R. B. H., & Hadjikhani, N. (2001). Where is "dorsal V4" in human visual cortex? Retinotopic, topographic and functional evidence. *Cerebral Cortex, 11,* 298–311.

Tootell, R. B., Hadjikhani, N., Hall, E. K., Marrett, S., Vanduffel, W., Vaughan, J. T., et al. (1998). The retinotopy of visual spatial attention. *Neuron, 21,* 1409–1422.

Tyler, C. W., Likova, L. T., Chen, C.-C., Kontsevich, L. L., & Wade, A. R. (2005). Extended concepts of occipital retinotopy. *Current Medical Imaging Reviews, 1,* 319–329.

Tyler, C. W., Likova, L. T., Kontsevich, L. L., & Wade, A. R. (2006). The specificity of cortical region KO to depth structure. *Neuroimage, 30,* 228–238.

Vuong, Q. C., Domini, F., & Caudek, C. (2006). Disparity and shading cues cooperate for surface interpolation. *Perception, 35,* 145–155.

Wagemans, J., van Doorn, A. J., & Koenderink, J. J. (2010). The shading cue in context. *i-Perception, 1,* 159–177.

Zeki, S., Perry, R. J., & Bartels, A. (2003). The processing of kinetic contours in the brain. *Cerebral Cortex, 13,* 189–202.

Zeki, S., Watson, J. D., Lueck, C. J., Friston, K. J., Kennard, C., & Frackowiak, R. S. (1991). A direct demonstration of functional specialization in human visual cortex. *Journal of Neuroscience, 11,* 641–649.